HU Protein Employs Similar Mechanisms of Minor-Groove Recognition in Binding to Different B-DNA Sites: Demonstration by Raman Spectroscopy†

Doinita Serban, James M. Benevides, and George J. Thomas, Jr.*

Division of Cell Biology and Biophysics, School of Biological Sciences, University of Missouri—Kansas City, Kansas City, Missouri 64110-2499

Received February 27, 2003; Revised Manuscript Received April 24, 2003

ABSTRACT: The sequence isomers d(CGCAAATTTGCG) and d(TCAAGGCCTTGA) form self-complementary duplexes that present distinct targets for binding of the homodimeric architectural protein HU of *Bacillus stearothermophilus* (HUBst). Raman spectroscopy shows that although each duplex structure is of the B-DNA type, there are subtle conformational dissimilarities between them, involving torsion angles of the phosphodiester backbone and the arrangements of stacked bases. Each DNA duplex forms a stable stoichiometric (1:1) complex with HUBst, in which the structure of the HUBst dimer is largely conserved. However, the Raman signature of each DNA duplex is perturbed significantly and similarly with HUBst binding, as reflected in marker bands assigned to localized vibrations of the phosphodiester moieties and base residues. The spectral perturbations identify a reorganization of the DNA backbone and partial unstacking of bases with HUBst binding, which is consistent with non-sequence-specific minor-groove recognition. Prominent among the HUBst-induced perturbations of B-DNA are a conversion of approximately one-third of the $\alpha/\beta/\gamma$ torsions from the canonical $g^-/t/g^+$ conformation to an alternative conformation, an equivalent conversion of deoxyadenosyl moieties from the C2′-*endo/anti* to the C3′-*endo/anti* conformation, and appreciable unstacking of purines. The results imply that each solution complex is characterized by structural perturbations extending throughout the 12-bp sequence. Comparison with previously studied protein/DNA complexes suggests that binding of HUBst bends DNA by approximately 70°.

The in vivo regulation of gene expression requires DNA interactions with both sequence-specific and nonspecific binding proteins. Available high-resolution structures suggest fundamental mechanistic differences between the two modes of binding (*1*−*4*). Characteristics of nonspecific binding include substantial conservation of the protein conformation, minor-groove attachment, and significant bridging of protein/DNA contacts by water molecules. Nonspecific recognition implies moderate binding affinity and is typically refractory to the stabilization of stoichiometric complexes, thus representing a potential obstacle to structure determination by high-resolution methods (*5*). In such cases, Raman spectroscopy can provide a convenient alternative approach for structure analysis.

In previous work, Raman difference spectroscopy has been exploited to identify vibrational signatures diagnostic of protein/DNA recognition in both sequence-specific and nonspecific complexes (*6*, *7*). The vibrational time scale relevant to Raman spectroscopy ($\sim 10^{-14}$ s) is favorable to direct sampling of the equilibrium population of the protein/DNA complex and constituents, irrespective of binding affinities in the subnanomolar range and relatively rapid dissociation kinetics. Here, we employ Raman difference spectroscopy to probe the molecular mechanism of DNA recognition by a versatile and nonspecific DNA-binding protein, the histone-like HU protein of *Bacillus stearothermophilus* (HUBst).[1] HUBst is a member of the broad and highly homologous family of dimeric HU proteins of eubacteria, which typically contain about 90 residues (∼10 kDa) per subunit (*8*). HU proteins function as architectural factors in replication initiation, posttranscriptional control, recombination, DNA repair, and chromosomal condensation (*8*−*12*).

Homodimeric HUBst exhibits essentially identical three-dimensional structures in both crystalline and solution states (*5*, *13*). However, like other HU proteins, no high-resolution structural information is available for its DNA complex. The subunit N-terminal domain of the DNA-free dimer consists of two α-helices, which are interleaved with corresponding α-helices of a partner subunit to form a four-helix platform. The C-terminal domain of each subunit forms a largely antiparallel β-stranded fold, which projects from the helix

† Part 82 in the series Raman Spectral Studies of Nucleic Acids. Supported by NIH Grant GM54378.

* To whom correspondence should be addressed. Tel: 816-235-5247. Fax: 816-235-1503. E-mail: thomasgj@umkc.edu.

[1] Abbreviations: EDTA, ethylenediaminetetraacetic acid; HMG, high mobility group; hSRY-HMG box, high-mobility-group box encoded by the male sex-determining region of the human Y chromosome; HUBst, protein HU from *Bacillus stearothermophilus*; IHF, integration host factor; LEF-1, lymphoid enhancer-binding factor 1; PAGE, polyacrylamide gel electrophoresis; TBE, Tris−borate−EDTA; Tris, tris(hydroxymethyl)aminomethane; α, P−O torsion angle defined by atoms O3′−P−O5′−C5′; β, O−C torsion angle defined by atoms P−O5′−C5′−C4′; γ, C−C torsion angle defined by atoms O5′−C5′−C4′−C3′; ζ, O−P torsion angle defined by atoms C3′−O3′−P−O5′. The colon symbol is employed, as in HUBst:DNA, to indicate a particular intermolecular complex.

10.1021/bi030050r CCC: $25.00
Published on Web 05/29/2003

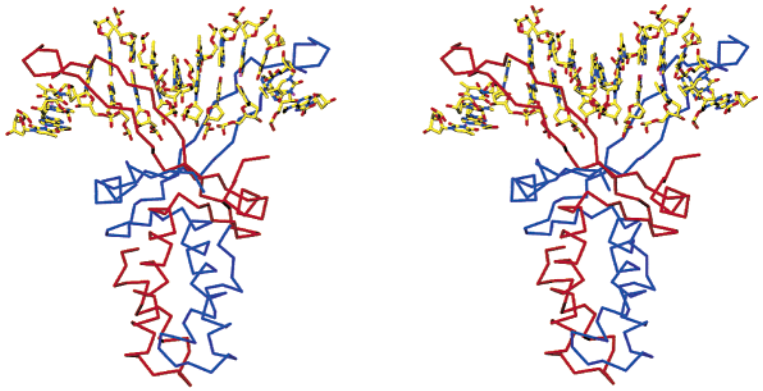

FIGURE 1: A hypothetical structure for the complex formed by HUBst and B-DNA, generated by fitting the three-dimensional solution structure of HUBst [NMR coordinates from PDB entry 1HUE (*5*)] with an idealized B-DNA target that is sharply bent at each of two minor-groove binding sites, leading to a cumulative helix bend angle of ~140°. The atomic structure of the complex is not known, although a much lower total DNA bend angle (~60−70°) has been proposed for HU from *E. coli* (*68*). Main-chain C^{α} atoms of HUBst dimer subunits are rendered in blue and red, and the DNA backbone is in yellow. Putative DNA-binding arms of HUBst subunits were fitted to the minor groove by homology modeling (http://us.expasy.org/sprot/) with the DNA-binding site of *E. coli* integration host factor (PDB entry 1IHF).

platform. The two C-terminal folds of the dimer do not interact with one another but diverge to form arms (β-arms) proposed as suitable for grasping the DNA double helix (*5*, *13*) (Figure 1). Biochemical and biophysical studies suggest that binding of HUBst to DNA induces a bend in the double helix with little or no apparent change in the protein structure (*5*). Similar results have been obtained for HU from *Escherichia coli* (*14*−*16*).

Despite the absence of a high-resolution structure for any HU:DNA complex, a model for HUBst/DNA recognition has been suggested by analogy with the crystal structure determined for a DNA complex of the *E. coli* integration host factor (IHF) (*17*). IHF, which exhibits both sequence-specific and nonspecific modes of DNA binding, shares 40% homology with HUBst and other HU proteins. The model proposed for the HUBst:DNA complex positions the β-arms of the dimer along the minor groove of B-DNA. The minor groove is widened by partial intercalation of proline and methionine side chains located at the end of each β-arm, and the DNA duplex is presumed to be significantly kinked or bent at the intercalation sites (*18*).

To gain a better understanding of the nature of HUBst/DNA recognition, we have employed Raman spectroscopy to compare the solution structures of complexes formed by HUBst with two dodecameric DNA sequence isomers, d(CGCAAATTTGCG) and d(TCAAGGCCTTGA), which are distinguished by their respective A/T- and G/C-rich central tracts. We also interpret Raman signatures of the protein-free dodecamers and show that they present conformationally distinct targets (although both are within the B-DNA family) for recognition by homodimeric HUBst. The present study identifies minor-groove recognition as the mechanism of HUBst binding to both DNA targets. The Raman results, which provide a new spectroscopic signature of minor-groove recognition, are discussed in relation to previously established Raman difference profiles of specific and nonspecific DNA binding.

MATERIALS AND METHODS

HUBst Expression. Recombinant HUBst was expressed in *E. coli* BL21(DE3)pLysS and purified according to described procedures (*19*, *20*). Protein concentration was determined by UV absorbance ($\epsilon_{258} = 0.076$ mL·mg^{-1}·cm^{-1} or 1482 M^{-1}·cm^{-1}) (*21*) using a Cary 3E spectrophotometer (Varian, Inc., Palo Alto, CA). The DNA-binding activity of the protein was established by circularization assays (*16*).

DNA Syntheses. The dodecameric sequence isomers, d(CGCAAATTTGCG) and d(TCAAGGCCTTGA), were synthesized on a Perspective Biosystems (Expedite) nucleic acid synthesizer using controlled pore glass supports and β-cyanoethyl phosphoramidite derivatives. The mass spectrum of each dodecamer (3642.5 ± 0.2 Da) was consistent with the sequence (3643 Da). Protocols for strand purification by HPLC (ISCO Model 2350) and resuspension in 0.1 M NaCl solution at pH 7.0 have been described (*22*). The self-complementary single strands were converted to duplexes by heating to 90 °C for 15 min in a dry bath, followed by slow cooling. After annealing, the solutions were dialyzed for several hours at 5 °C against 2 M NaCl and 1 mM EDTA solution. Dialysis was continued for an additional 24 h against several changes of distilled water. Following dialysis, each DNA duplex solution was lyophilized, and the lyophilizate was stored at −20 °C. The extinction coefficient at 260 nm for each duplex ($\epsilon_{260} = 112.5$ mM^{-1}·cm^{-1}) was calculated from available data (*23*, *24*).

Identical dodecamers, labeled with the fluorescent dye Oregon Green 488, were purchased from Molecular Probes, Eugene, OR. The mass spectrum of each labeled strand (4333.7 ± 1.5 Da) was consistent with the labeled sequence (4333 Da). Stock solutions (140 μM) in sample buffer (10 mM Tris, 50 mM NaCl, pH 7.5) were stored at −20 °C. Concentrations of dye-labeled DNA solutions were determined from the extinction coefficient ($\epsilon_{260} = 160.5$ mM^{-1}·cm^{-1}) provided by the vendor.

Nondenaturing Polyacrylamide Gel Electrophoresis (PAGE). Aliquots of stock solutions of HUBst and labeled DNA in sample buffer were mixed at specific molar ratios in the range 1:4 < HUBst:DNA < 1:1 to a final volume of ~10 μL and were incubated at 15 °C for 15 min. For electrophoresis experiments, the DNA concentration (14 μM) was maintained higher than the estimated K_d values governing HU binding to undistorted (<2.5 μM) and distorted (0.002 μM) duplexes (*56*, *68*). A 2 μL aliquot of dye solution (15% glycerol, 0.05% bromophenol blue) was added to each sample, and

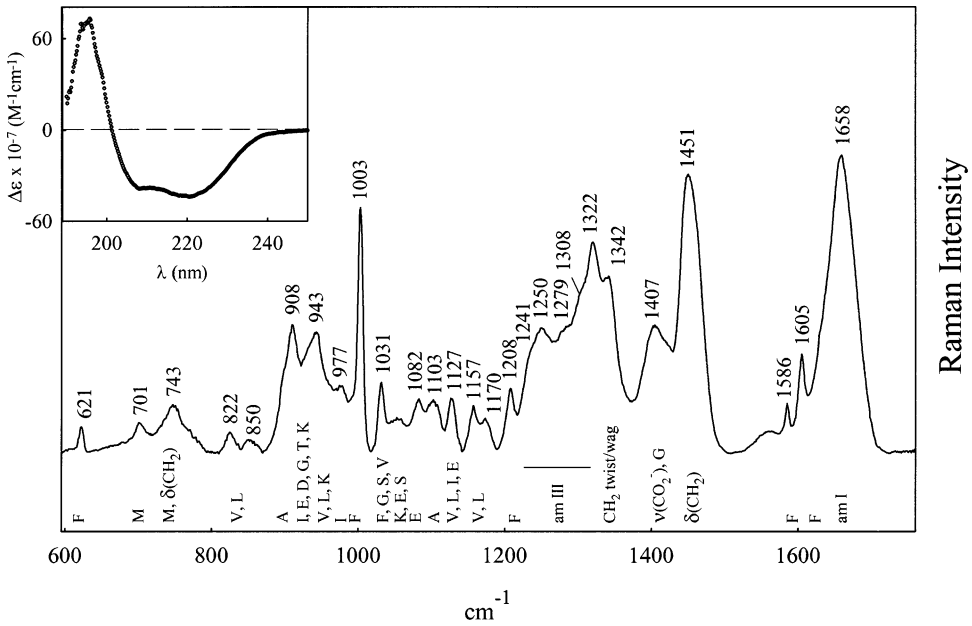

FIGURE 2: Raman spectrum in the region 600−1800 cm^{-1} obtained by 532 nm excitation of HUBst (20 μg/μL in 10 mM Tris and 50 mM NaCl, pH 7.5, solution). Wavenumber labels identify prominent Raman bands discussed in the text. Raman band assignments to amino acid (one-letter abbreviations) or amide (am) vibrations, which are listed along the abscissa, are from ref *20*. The CD spectrum of HUBst (~0.3 mg/mL) is shown in the insert at the upper left. Raman and CD data were obtained at 20 °C.

PAGE was conducted on 8% gels in TBE buffer (4.5 mM Tris, 4.5 mM boric acid, 0.1 mM EDTA, pH 8.0) for 4 h at 110 V and 4 °C. Fluorescent DNA bands were visualized using a Storm Imager (model 810, Molecular Dynamics, Inc.) and quantified using Image Quant software (Molecular Dynamics, Inc., version 4.2). The fractions of unbound and protein-bound DNA in a given lane were determined from the areas of the respectively assigned bands, and the total amount of DNA in the lane was computed from the sum of band areas. Comparisons between lanes were made after normalization of the band areas of a given lane to the total amount of DNA in that lane.

Raman Spectroscopy. Raman spectra were obtained on solutions of HUBst (20 μg/μL ≈ 1 mM dimer), DNA (40 μg/μL ≈ 5.5 mM duplex), and their equimolar complex (HUBst:DNA), each in sample buffer. The HUBst:DNA complex was prepared by dissolving the lyophilized protein in 5.5 mM DNA solution in sample buffer. Samples of approximately 5 μL volume were sealed in glass capillaries (KIMAX No. 34507) and mounted in the thermostated (20 °C) sample illuminator of the Raman spectrophotometer (*25*). Spectra were excited at 532 nm using a solid-state Nd:YVO_4 laser (Verdi, Coherent, Inc., Santa Clara, CA). Raman scattering at 90° was collected on a Spex 500 M single spectrograph (Horiba Group, Instruments S.A., Edison, NJ), equipped with a holographic notch filter and liquid-nitrogen cooled, back-thinned, charge-coupled-device detector of 2000 × 800 pixels (Spectrum One, Instruments S.A.). The radiant power at the sample was approximately 30 mW. The effective spectral resolution was 3 cm^{-1}. Raman frequencies, accurate to ±0.5 cm^{-1}, were calibrated using the 459.5 cm^{-1} band of CCl_4. Spectra shown below are the accumulated averages of 10−30 exposures of 40 s each. Further details of the instrumentation and data collection protocols are given elsewhere (*26*).

Circular Dichroism Spectroscopy. CD spectra of HUBst solutions (~0.3 mg/mL in 1 mM sodium cacodylate buffer, pH 7.0, 20 °C) were obtained on a Jasco J-720 spectropolarimeter (Japan Spectroscopic Co., Tokyo) using an optical path of 0.1 cm. The spectropolarimeter was calibrated with ammonium *d*-camphor-10-sulfonate. CD data referenced below represent the accumulated averages of five scans, each obtained at a scan rate of 0.5 nm/s.

RESULTS AND INTERPRETATION

Raman Signature of HUBst. The Raman spectrum of HUBst (Figure 2) is distinguished by a strong and broad amide I band centered at 1658 cm^{-1} and a complex amide III profile, which includes a major peak at 1250 cm^{-1} and weaker shoulders at approximately 1241, 1279, and 1308 cm^{-1}. Previous analysis of the Raman amide markers shows that the HUBst solution structure comprises 36 ± 2% α-helix, 25 ± 3% β-strand, and 38 ± 3% irregular conformations (*20*), in accord with the CD profile (Figure 2, insert) and the NMR solution structure (*5*). Other major contributors to the Raman signature of HUBst are the subunit Phe (4), Ala (12), and Arg (5) side chains, which generate several prominent bands as labeled in Figure 2 (*20*). Because HUBst contains neither Trp nor Tyr, its Raman spectrum is free of the otherwise intense bands expected from these aromatic side chains in the intervals 750−900, 1350−1400, and 1550−1600 cm^{-1}, thus facilitating the detection and quantification of key nucleotide markers in Raman spectra of HUBst:DNA complexes.

Raman Signatures of d(CGCAAATTTGCG) and d(TCAAGGCCTTGA) Duplexes. Figure 3 compares Raman spectra of duplexes formed by the self-complementary dodecamers d(CGCAAATTTGCG) (top trace) and d(TCAAGGCCTTGA) (middle trace). Labels along the abscissa identify bands assigned to localized vibrations of either specific base residues (A, C, G, T) or the deoxyribosyl-phosphate backbone (bk). The data indicate primarily C2′-*endo/anti* deoxynucleosides, *gauche*$^-$ (g^-) conformations for the phosphodiester torsion angles α and ζ, and predominantly stacked

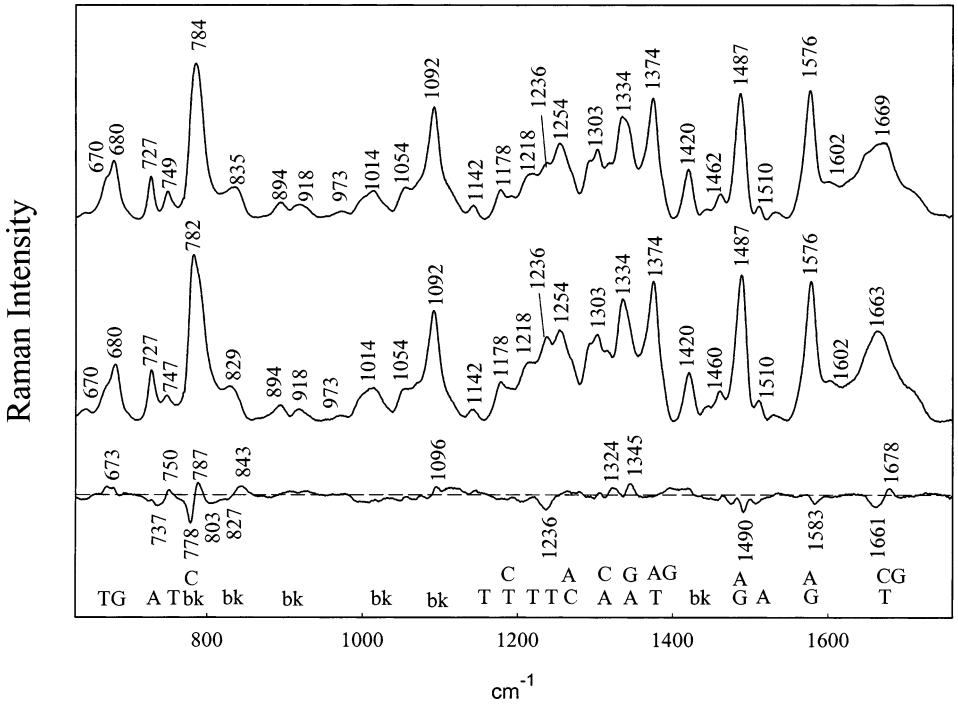

FIGURE 3: Raman spectra (600−1800 cm^{-1}, 532 nm excitation) of d(CGCAAATTTGCG) (trace A) and d(TCAAGGCCTTGA) (trace B) duplexes, each at 40 μg/μL in 10 mM Tris and 50 mM NaCl, pH 7.5, solution, and their difference spectrum (trace C = trace A − trace B). Spectra were normalized to the integrated intensity of the phosphate Raman band at 1092 cm^{-1}, which is independent of base composition (*31*).

base pairs. The basis for these assignments and interpretations has been given in previous papers (*27*−*30*). Figure 3 demonstrates that although the two dodecamers adopt similar B-DNA structures, they differ in conformational detail. The nature of the structural differences can be inferred from the Raman difference bands of Figure 3 (bottom trace), which are interpreted as follows.

The difference peak at 843 cm^{-1} and trough at 803 cm^{-1} reflect parent bands centered respectively at 835 cm^{-1} in d(CGCAAATTTGCG) and 829 cm^{-1} in d(TCAAGGCCTTGA) and indicate different average backbone conformations in the two DNAs. Similar differences have been observed between AT-rich and GC-rich genomic DNAs and attributed to differences in minor-groove dimensions (*27*, *30*, *31*). The data of Figure 3 thus suggest that the minor groove of d(CGCAAATTTGCG) is narrower than that of d(TCAAGGCCTTGA) and may be more favorable to the organization of water molecules as proposed previously for $(dA)_n \cdot (dT)_n$ tracts (spine of hydration) (*32*−*35*). The present Raman results imply that conformational details of the two dodecamers are strongly influenced by the base pairs comprising their central segments.

The difference peak at 787 cm^{-1} and trough at 778 cm^{-1} originate from differences in either or both of the two contributors to the very intense and broad band centered at 784 cm^{-1} in d(CGCAAATTTGCG) and 782 cm^{-1} in d(TCAAGGCCTTGA). The contributors are a cytosine ring marker at ∼780 cm^{-1} and a backbone conformation marker at ∼790 cm^{-1} (*30*). The intensity of the former is expected to increase modestly with cytosine unstacking (hypochromism), whereas the latter is highly sensitive in both intensity and wavenumber to torsions of the DNA backbone (α, β, γ, ζ). Because both duplexes are largely base paired and stacked, differences in Raman hypochromism at 780 cm^{-1} should be small. Accordingly, we attribute the observed 787/778 cm^{-1} difference features primarily to different average backbone conformations in the two DNAs. This is consistent with the interpretation given above for the 843/803 cm^{-1} difference features.

The difference peak near 673 cm^{-1} and relative minimum/maximum at 737/750 cm^{-1}, as well as difference features between 1200 and 1700 cm^{-1}, all coincide with Raman markers of base residues and reflect the distinct sequence-directed base stacking interactions of the two duplexes. Thymine and adenine residues are significant contributors to the majority of these difference bands (*28*), including those at 673, 737/750, 1236, 1324, 1345, 1490, 1661, and 1678 cm^{-1} (*26*, *36*). Because all dT residues of d(CGCAAATTTGCG) are centrally located and stably paired and stacked at the experimental conditions employed, the differences in dT Raman markers could reflect partial fraying of the terminal A·T pairs of d(TCAAGGCCTTGA). Unstable terminal pairs may also account for the troughs at 1236 and 1661 cm^{-1} (*37*). Subtle deoxynucleoside conformational differences and sequence-specific base stacking geometries may also contribute to the features at 673 (dT, dG) and 737/750 cm^{-1} (dA, dT). The relatively high amplitudes of the troughs at 1490 (primarily dG) and 1583 (both dA and dG) cm^{-1} reflect contributions from both adenines and guanines. The apparently different purine hypochromism in the two duplexes implies that the purines are more effectively stacked in d(CGCAAATTTGCG). This is surprising, given the more polypurine-like environment of A and G in the d(TCAAGGCCTTGA) sequence.

The well-characterized Raman markers of C2′-*endo/anti* dG (680 cm^{-1}), dA (727 cm^{-1}), and dC (1254 cm^{-1}) (*30*) make no significant contributions to the difference spectrum

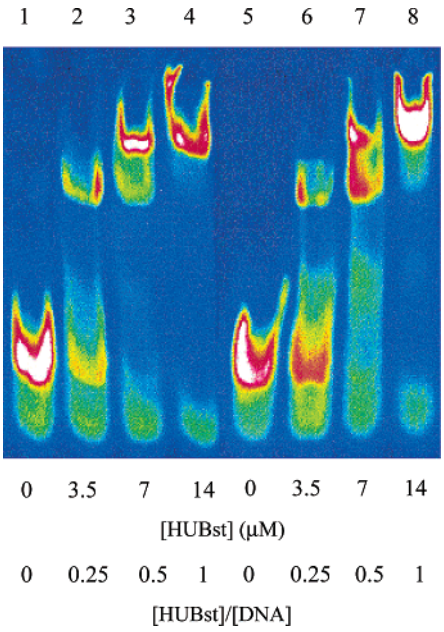

FIGURE 4: Gel mobility shift assay of complexes formed in mixtures of HUBst with dye-labeled DNAs, d(CGCAAATTTGCG) (lanes 2−4) and d(TCAAGGCCTTGA) (lanes 6−8). Corresponding protein-free DNAs are in lanes 1 and 5. The nominal concentration of labeled DNA in each lane was constant (∼14 μM). HUBst concentrations (μM) and HUBst:DNA molar ratios are as indicated along the bottom axis. Further details regarding quantification and normalization procedures are discussed in the text.

of Figure 3, indicating that deoxynucleoside conformations are essentially the same in the two duplexes.

Characterization of HU:DNA Complexes by Agarose Gel Electrophoresis. Figure 4 shows a semiquantitative gel mobility analysis of dye-labeled d(CGCAAATTTGCG) (lane 1) and d(TCAAGGCCTTGA) (lane 5) and complexes formed by HUBst with these DNAs (lanes 2−4 and 6−8, respectively). Lanes 1 and 5 demonstrate that, as expected, the two dodecamer duplexes exhibit similar electrophoretic mobilities in the absence of HUBst. Lanes 4 and 8 indicate that for each duplex a single and highly homogeneous complex is obtained in the presence of an equimolar concentration of HUBst dimer. [The Raman spectra shown below were obtained from complexes formed in equimolar HUBst:DNA solutions (5.5 mM), corresponding to the protein:DNA ratios of lanes 4 and 8.] At intermediate HUBst-to-DNA ratios, viz., lanes 2 and 3 for d(CGCAAATTTGCG) and lanes 6 and 7 for d(TCAAGGCCTTGA), we find evidence of a distinctive precursor complex for each dodecamer. In addition, different relative proportions of the precursor and equimolar complexes are formed for the two sequences (cf. lanes 3 and 7). Specifically, lane 3 of Figure 4 suggests that, for the solution containing the 0.5:1.0 molar ratio of HUBst:d(CGCAAATTTGCG), the equimolar complex predominates (∼65%) over the precursor (<25%). Conversely, lane 7 indicates that, for d(TCAAGGCCTTGA), the precursor and equimolar complexes are present in roughly equal proportions (∼30%). All lanes of Figure 4 exhibit a weak and diffuse background at the bottom of the gel, suggesting a small percentage (∼10%) of free dye (Oregon Green 488), which is believed to reflect the low level of hydrolysis expected of the labeled DNA.

Similar precursor complexes have been reported in previous gel mobility analyses of the binding of HU proteins to

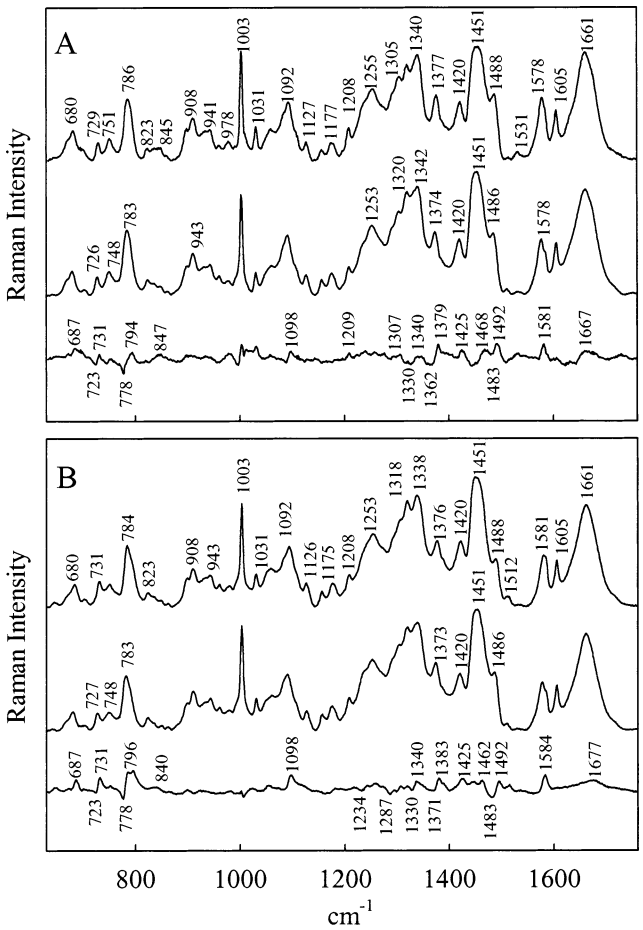

FIGURE 5: Panel A: Raman spectrum of the equimolar HUBst:d(CGCAAATTTGCG) complex (top trace), the spectral sum of constituents, HUBst + DNA (middle trace), and their digital difference (bottom trace). Panel B: Raman spectrum of the equimolar HUBst:d(TCAAGGCCTTGA) complex (top trace), the spectral sum of constituents, HUBst + DNA (middle trace), and their digital difference (bottom trace). Experimental conditions are as given in the legends of Figures 2 and 3.

longer DNA sequences (*14*, *38*, *39*). At present, no definitive structural information is available on any HU:DNA complex, although the previously reported electrophoretic results have been attributed to the presence of topological variants of protein-bound DNA.

Characterization of DNA Structure Changes from Raman Spectra of HUBst:DNA Complexes. The Raman spectrum of the 1:1 complex of HUBst with d(CGCAAATTTGCG) is compared with the spectral sum of constituents in panel A of Figure 5. The difference spectrum computed between complex and constituents (bottom trace) exhibits numerous peaks and troughs demonstrating significant conformational changes to the DNA target with complex formation. Corresponding data for the complex of HUBst with d(TCAAGGCCTTGA) are shown in panel B of Figure 5. The two difference spectra of Figure 5 are strikingly similar to one another, both in the positions of their peaks and troughs and in the corresponding difference amplitudes. It is clear that both DNAs suffer similarly large structural perturbations with binding of HUBst. The nature of these protein-induced structural changes is revealed by the affected Raman markers, as follows.

(1) Conformations and Environments of DNA Phosphates. Prominent peak/trough features within the 770−800 cm^{-1}

intervals of the Figure 5 difference spectra indicate similar conformational perturbations to the C5′−O5′−P−O3′−C3′ backbone networks of both DNAs upon HUBst binding. In each case the peak/trough feature, which represents ∼33% of the parent band intensity, reflects an HUBst-induced shift to a lower wavenumber of the band center. As noted previously (*6*, *7*), such a wavenumber shift reflects a change in the average backbone torsion angles, α (O3′−P−O5′−C5′), β (P−O5′−C5′−C4′), and γ (O5′−C5′−C4′−C3′), from the $g^-/t/g^+$ range to the *t*/*t*/*t* range. Consistent with this interpretation is a difference peak exhibited near 840−850 cm^{-1} for each complex (*40*). Both difference spectra of Figure 5 also exhibit a difference peak near 1098 cm^{-1}, which reflects broadening of the parent phosphodioxy (PO_2^-) Raman marker upon HUBst binding and signals a change in local electrostatic environment of the DNA phosphates. Similar broadening of the Raman phosphodioxy marker accompanies electrostatic shielding of DNA phosphates by divalent metal ions (*41*−*44*).

(2) Deoxyribosyl Conformations. In addition to HUBst-induced changes in DNA phosphodiester geometry and phosphodioxy environment, furanose ring conformations of the deoxynucleotides are also altered by protein binding. The trough/peak features at 723/731 and near 1330/1340 cm^{-1} are consistent with small net changes in dT and dA conformations from the C2′-*endo/anti* to C3′-*endo/anti* ranges. Similar Raman marker shifts accompany the canonical B- to A-DNA transition (*45*−*48*). Additional spectral evidence of perturbed deoxyribosyl conformations is provided by the Raman difference peaks near 1425 and 1465 cm^{-1}, which reflect broadening of the parent C5′H_2 and C2′H_2 marker bands of DNA near 1420 and 1462 cm^{-1}, respectively (*26*, *37*, *49*, *50*). [Note that the latter is eclipsed in the parent spectra of Figure 5 by the more intense 1451 cm^{-1} marker originating from the CH_2 groups of HUBst side chains (*20*).] Nevertheless, the observed DNA difference peaks represent a significant fraction of the parent band intensities (e.g., ∼25−50% for the 1420 cm^{-1} marker) and imply that three to six deoxynucleotides of each dodecamer strand suffer conformational perturbations to furanose moieties (*6*, *7*, *31*, *49*, *51*).

(3) Purine Environments. In addition to reorganizations of the DNA backbone, HUBst binding perturbs DNA base environments. The relative minimum/maximum near 1483/1492 cm^{-1} in each difference spectrum of Figure 5 suggests weaker N7 hydrogen bonding in the complex than in the protein-free DNA (*52*−*54*). Changes in purine base-stacking environments and/or deoxynucleoside conformations with HUBst binding also contribute to these difference features, as well as to the difference peaks at 687 (dG) and 731 cm^{-1} (dA) and near 1581−1584 cm^{-1} (*30*).

(4) Pyrimidine Environments. Thymine residues of B-DNA generate a Raman marker near 1375−1380 cm^{-1}, which gains intensity with increasing hydrophobicity of the C5H_3 environment (*6*, *40*). The difference peak near 1380 cm^{-1} in each difference spectrum of Figure 5 indicates an increase in the average hydrophobicity of thymine C5H_3 groups upon complex formation. A similar effect occurs for specific complex formation between a DNA octamer and a high mobility group of the human sex-determining factor (hSRY-HMG) (*6*). The present results suggest that both the nonspecific HUBst:DNA complexes and the specific hSRY-HMG:DNA complex share this Raman signature feature. The small difference peak near 1660−1670 cm^{-1} in each complex also identifies HUBst-induced perturbations to thymines. This may reflect altered hydrogen bonding of dT exocyclic carbonyls (*37*).

DISCUSSION AND CONCLUSIONS

Mechanism of HUBst Recognition of DNA. Raman difference spectroscopy of complexes formed between HUBst and the two DNA dodecamers, d(CGCAAATTTGCG) and d(TCAAGGCCTTGA), indicates significant changes to the B-form backbone of each DNA as a direct consequence of HUBst binding. For each complex we observe the conversion of roughly one-third of α/β/γ phosphodiester torsions from the $g^-/t/g^+$ to the *t*/*t*/*t* conformation and an equivalent deoxyribosyl conformational change in dA residues from C2′-*endo/anti* to C3′-*endo/anti*. Evidence for partial unstacking of purines is also observed. The similarity of structural perturbations for the two DNA targets indicates a non-sequence-specific mechanism of HUBst/DNA recognition.

The two DNA targets employed here differ not only in sequence but also in details of secondary structure, as revealed by distinctive Raman signatures in the absence of protein (Figure 3). Importantly, the structural perturbations suffered by each DNA as a consequence of HUBst binding are much greater (more than 2-fold) than the differences observed between their protein-free Raman signatures (cf. Figures 3 and 5). We conclude that nuances of secondary structure that distinguish the two B-DNA dodecamers do not significantly affect HUBst recognition. The present data demonstrate that purine Raman markers of the d(CGCAAATTTGCG) and d(TCAAGGCCTTGA) dodecamers also exhibit large and comparable perturbations with HUBst interaction. Because the purines are distributed differently along the two DNA sequences, the results suggest that HUBst-induced structural perturbations are not restricted to the side-chain intercalation sites.

While the effects of HUBst binding on DNA dodecamer conformation appear to be more "global" than "local", the Raman results do not provide further insight into the detailed structures of the complexes. At present, no high-resolution structure exists for any HU/DNA complex. Therefore, it is not possible to assess the present results in connection with an experimentally determined structural mechanism. However, both prolyl and methionyl side-chain intercalations (Pro 72, Met 69) have been considered as plausible mechanisms for HUBst/DNA recognition, analogous to the side-chain intercalation mechanism determined for the X-ray crystal structure of IHF:DNA (*17*). On the other hand, the available IHF:DNA structure is that of a sequence-specific complex, which may involve a mode of protein/DNA interaction distinct from that required for non-sequence-specific recognition.

Previous studies have demonstrated that HU proteins generally bind less prolifically to uniformly double-helical B-DNA than to deformed DNAs (including duplexes containing nicks or gaps, cruciforms, and supercoils) (*8*, *15*, *55*, *56*). The gel mobility shift analysis of Figure 4 suggests a modestly greater affinity of HUBst for d(CGCAAATTTGCG) than for d(TCAAGGCCTTGA). This may be indicative of a more significant departure of the former duplex from a uniform B-helix.

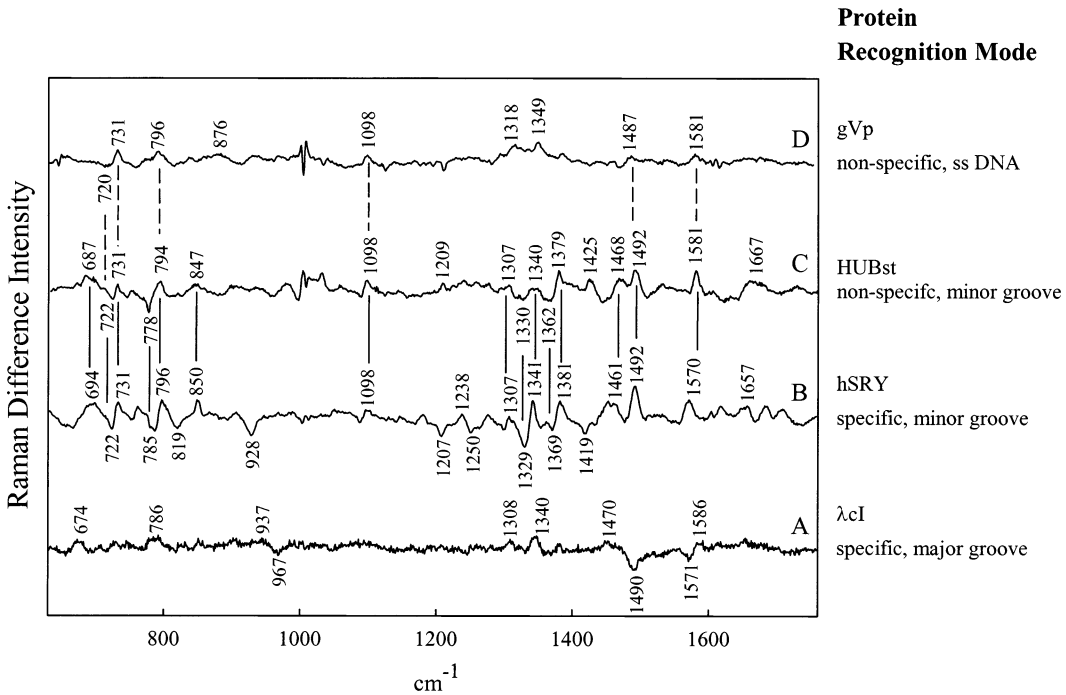

FIGURE 6: From bottom to top: Raman difference signatures indicating DNA structure reorganizations produced by binding of (A) the N-terminal domain of phage λ cI repressor to the O_L1 site (specific major-groove recognition) (*40*), (B) the hSRY-HMG box to d(GAACAATC)·d(GATTGTTC) (specific minor-groove recognition) (*6*, *7*), (C) the HUBst dimer to $[d(CGCAAATTTGCG)]_2$ (non-sequence-specific minor-groove recognition), and (D) the gene V protein of M13 to poly(dA) (non-sequence-specific ssDNA recognition) (*69*). Data have been scaled to the intensity of the 1092 cm^{-1} band of the DNA phosphate group in the parent spectra, as described previously (*6*).

The structural adjustment of DNA to HUBst binding occurs with little or no apparent consequences to HUBst conformation, suggesting an induced-fit mechanism. This is consistent with the highly stable secondary structure of HUBst that is confirmed by both NMR (*5*) and H/D exchange studies (*20*).

Comparison with Raman Signatures of Other Protein/DNA Complexes. The Raman difference spectrum diagnostic of HUBst-dependent reorganization of DNA (Figure 5) constitutes a spectroscopic signature for non-sequence-specific B-DNA recognition. It is of interest to compare this signature with those reported for other modes of protein/DNA recognition investigated by Raman spectroscopy. Figure 6 illustrates comparisons with sequence-specific minor-groove recognition (hSRY-HMG:DNA), sequence-specific major-groove recognition (λ cI:DNA), and non-sequence-specific ssDNA recognition [gVp:poly(dA)].

Figure 6 demonstrates striking similarities between the Raman difference signatures of HUBst:DNA and hSRY-HMG:DNA recognition. These similarities, which are connected by the solid vertical lines in the figure and which represent parent bands originating not only from the deoxyribosyl−phosphate backbone but also from purine and pyrimidine base residues (see assignments indicated in Figure 3), provide strong evidence in favor of similar molecular mechanisms of binding. Accordingly, we conclude that HUBst, like hSRY-HMG (*57*), binds its DNA target along the minor groove. It is interesting that the similarities noted above between the Raman difference signatures of HUBst:d(CGCAAATTTGCG) and HUBst:d(TGAAGGCCTTCA) recognition (Figure 5) extend also to hSRY-HMG:DNA. We propose that these common minor-groove binding mechanisms also involve similar hydrophobic side-chain intercalations, despite the distinctly different folds of the respective proteins. A corollary to the present results is that the Raman difference signature for minor-groove recognition is not highly sensitive to (i) the sequence of the DNA target site or (ii) the fold of the protein recognition domain. Structural studies of other minor-groove complexes include proteins that bind DNA specifically (IHF, LEF-1) and nonspecifically (HMG1, HMG 2). Consistent with the present results, these exhibit similar molecular mechanisms of DNA recognition and DNA structure perturbation, irrespective of the sequence specificity of binding (*17*, *58*−*60*). All induce base unstacking and bending of the DNA helix at two sites separated by eight or more base pairs, and all involve partial intercalation of protein aliphatic side chains.

A Model for HU/DNA Recognition. Footprinting studies of complexes of high-molecular-weight DNA with the HU protein from *E. coli* indicate positioning of the protein β-arms along the DNA minor groove (*61*). Gel mobility shift assays imply appreciable bending of DNA by the bound protein (*14*, *16*, *38*, *62*). The present results provide further experimental support for this mode of binding and, in addition, reveal many of the details of B-DNA structure perturbation attendant with complex formation, as has been noted above. Although the observed Raman difference features do not provide direct information about the average bending angle of the HUBst-bound DNA, the similarity between Raman difference profiles of HUBst:DNA and hSRY-HMG:DNA complexes (Figure 6) suggests similarly distorted DNA structures, i.e., an overall bend of approximately 70° in the DNA helix axis.

We emphasize that the present study does not provide direct information on either the location of the HUBst-induced kinks that bend the DNA helix or the precise magnitude of the bend angle. Two possible limiting cases, which are depicted schematically in Figure 7, are relatively

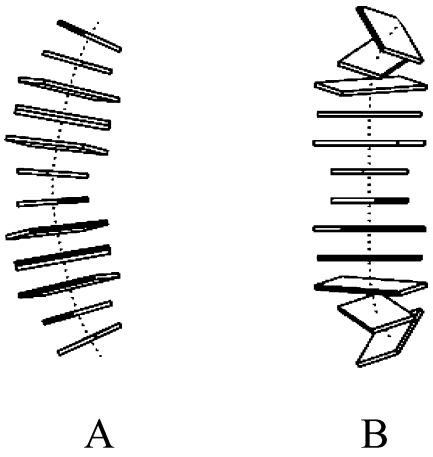

FIGURE 7: Two possible limiting cases for DNA bending by the HUBst protein. In (A) the continuously curved helix axis results from a phased series of delocalized low-amplitude kinks. In (B) a sharply bent helix axis results from two high-amplitude kinks localized at the putative sites of HUBst side-chain intercalation. The Raman results do not distinguish rigorously between the possibilities illustrated here but favor either (A) or an intermediate between (A) and (B) in which the DNA structural perturbations are largely delocalized. A scenario similar to (B) is supported by the crystal structure of a complex between the *Anabena* HU protein and a 20-bp DNA fragment incorporating both unpaired and mismatched thymines (P. Rice, personal communication). Models are based on SCHNArP software, courtesy of Dr. Xiang-Jun Lu.

smooth helix curvature resulting from a phased series of low-amplitude kinks (Figure 7A) and a more sharply bent helix axis resulting from higher amplitude kinks localized at the HUBst side-chain intercalation sites (Figure 7B). The Raman results do not distinguish between these possibilities, or intermediate scenarios, as long as the backbone reorganization perturbs only about one-third of the phosphodiester band intensity and the altered base stacking is propagated through much of the dodecamer. In this regard it should be noted that the cartoon of Figure 1, which represents a conjunction of the HUBst dimer crystal structure (*13*) with the DNA fragment in the crystal structure of the IHF:DNA complex (*17*), reflects a larger DNA bend angle (~140°) than suggested by the Raman results. An HU-induced bend angle of lesser magnitude (~105°) has been proposed by Rice and co-workers (P. Rice, personal communication), who recently solved the crystal structure of a complex of the *Anabena* HU protein with a 20-bp DNA fragment incorporating both unpaired and mismatched thymines. Thus, the X-ray structure of the *Anabena* HU:DNA complex and the Raman results on two HUBst:DNA complexes in solution favor smaller DNA bend angles than determined for IHF:DNA. It seems likely that the degree of bending suffered by DNA targets in complexes with HU proteins may differ according to the base sequence, regularity of the duplex, and local molecular environment. Crystal packing and hydration effects may also be significant factors in determining structural details of the complexes. This view is consistent with the diverse roles of HU proteins and the highly dynamic nature of HU:DNA binding (*15*, *56*, *63*, *64*).

Future Prospects. The present findings demonstrate a Raman signature diagnostic of nonspecific B-DNA minor-groove recognition. The results establish a framework for subsequent exploitation of this Raman fingerprint to probe the roles of HU and related architectural proteins in manipulating larger DNA constructs, such as plasmids and genomic DNAs. Future work will also focus on the application of ultraviolet−resonance Raman spectroscopy to HUBst:DNA complexes in order to investigate by 229 nm excitation the structure-sensitive Raman signals of the putative intercalating residue, Pro 72 (*20*), and by 257 nm excitation those of the DNA intercalation sites (*65*).

The present experimental design has targeted DNA dodecamers containing purine/pyrimidine steps at the most probable HUBst side-chain intercalation sites [d(CGCAAATTTGCG) and d(TCAAGGCCTTGA)]. Purine/pyrimidine steps have been identified previously as readily inducible bending loci in protein:DNA complexes (*22*, *66*, *67*). It will be of interest to compare the present results with those obtained in studies of complexes not containing such purine/pyrimidine steps.

Finally, we note that the extension of this methodology to corresponding IHF:DNA complexes should also provide insights into structural factors differentiating specific and nonspecific modes of minor-groove recognition.

ACKNOWLEDGMENT

D.S. thanks Prof. Marilyn D. Yoder (UMKC) for assistance with computer modeling and data analysis. The authors thank Prof. Phoebe A. Rice (University of Chicago) for sharing results on the crystal structure of an HU:DNA complex prior to publication and for many helpful discussions and Prof. Constantinos E. Vorgias (National and Kapodistrian University of Athens) for providing the HUBst expression system.

REFERENCES

1. Burley, S. K., Xie, X., Clark, K. L., and Shu, F. (1997) Histone-like transcription factors in eukaryotes, *Curr. Opin. Struct. Biol. 7*, 94−102.
2. Murphy, F. V., Sweet, R. M., and Churchill, M. E. (1999) The structure of a chromosomal high mobility group protein-DNA complex reveals sequence-neutral mechanisms important for non-sequence-specific DNA recognition, *EMBO J. 18*, 6610−6618.
3. Su, S., Gao, Y. G., Robinson, H., Liaw, Y. C., Edmondson, S. P., Shriver, J. W., and Wang, A. H. (2000) Crystal structures of the chromosomal proteins Sso7d/Sac7d bound to DNA containing T-G mismatched base-pairs, *J. Mol. Biol. 303*, 395−403.
4. Huffman, J. L., and Brennan, R. G. (2002) Prokaryotic transcription regulators: More than just the helix-turn-helix motif, *Curr. Opin. Struct. Biol. 12*, 98−106.
5. Boelens, R., Vis, H., Vorgias, C. E., Wilson, K. S., and Kaptein, R. (1996) Structure and dynamics of the DNA binding protein HU from *Bacillus stearothermophilus* by NMR spectroscopy, *Biopolymers 40*, 553−559.
6. Benevides, J. M., Chan, G., Lu, X. J., Olson, W. K., Weiss, M. A., and Thomas, G. J., Jr. (2000) Protein-directed DNA structure. I. Raman spectroscopy of a high-mobility-group box with application to human sex reversal, *Biochemistry 39*, 537−547.
7. Benevides, J. M., Li, T., Lu, X. J., Srinivasan, A. R., Olson, W. K., Weiss, M. A., and Thomas, G. J., Jr. (2000) Protein-directed DNA structure. II. Raman spectroscopy of a leucine zipper bZIP complex, *Biochemistry 39*, 548−556.
8. Drlica, K., and Rouviere-Yaniv, J. (1987) Histonelike proteins of bacteria, *Microbiol. Rev. 51*, 301−319.
9. Rice, P. A. (1997) Making DNA do a U-turn: IHF and related proteins, *Curr. Opin. Struct. Biol. 7*, 86−93.
10. Bewley, C. A., Gronenborn, A. M., and Clore, G. M. (1998) Minor groove-binding architectural proteins: Structure, function, and DNA recognition, *Annu. Rev. Biophys. Biomol. Struct. 27*, 105−131.
11. Segall, A. M., Goodman, S. D., and Nash, H. A. (1994) Architectural elements in nucleoprotein complexes: Interchange-

ability of specific and non-specific DNA binding proteins, *EMBO J. 13*, 4536−4548.
12. Dri, A. M., Moreau, P. L., and Rouviere-Yaniv, J. (1992) Role of the histone-like proteins OsmZ and HU in homologous recombination, *Gene 120*, 11−16.
13. White, S. W., Wilson, K. S., Appelt, K., and Tanaka, I. (1999) The high-resolution structure of DNA-binding protein HU from *Bacillus stearothermophilus*, *Acta Crystallogr., Sect. D: Biol. Crystallogr. 55* (Part 4), 801−809.
14. Wojtuszewski, K., Hawkins, M. E., Cole, J. L., and Mukerji, I. (2001) HU binding to DNA: Evidence for multiple complex formation and DNA bending, *Biochemistry 40*, 2588−2598.
15. Kobryn, K., Lavoie, B. D., and Chaconas, G. (1999) Supercoiling-dependent site-specific binding of HU to naked Mu DNA, *J. Mol. Biol. 289*, 777−784.
16. Hodges-Garcia, Y., Hagerman, P. J., and Pettijohn, D. E. (1989) DNA ring closure mediated by protein HU, *J. Biol. Chem. 264*, 14621−14623.
17. Rice, P. A., Yang, S., Mizuuchi, K., and Nash, H. A. (1996) Crystal structure of an IHF-DNA complex: A protein-induced DNA U-turn, *Cell 87*, 1295−1306.
18. White, S. W., Appelt, K., Wilson, K. S., and Tanaka, I. (1989) A protein structural motif that bends DNA, *Proteins 5*, 281−288.
19. Padas, P. M., Wilson, K. S., and Vorgias, C. E. (1992) The DNA-binding protein HU from mesophilic and thermophilic bacilli: Gene cloning, overproduction and purification, *Gene 117*, 39−44.
20. Serban, D., Arciniegas, S. F., Vorgias, C. E., and Thomas, G. J., Jr. (2003) Structure and dynamics of the DNA-binding protein HU of *B. stearothermophilus* investigated by Raman and ultraviolet-resonance Raman spectroscopy, *Protein Sci. 12*, 861−870.
21. Welfle, H., Misselwitz, R., Welfle, K., Groch, N., and Heinemann, U. (1992) Salt-dependent and protein-concentration-dependent changes in the solution structure of the DNA-binding histone-like protein, HBsu, from *Bacillus subtilis*, *Eur. J. Biochem. 204*, 1049−1055.
22. Benevides, J. M., Kukolj, G., Autexier, C., Aubrey, K. L., DuBow, M. S., and Thomas, G. J., Jr. (1994) Secondary structure and interaction of phage D108 Ner repressor with a 61-base-pair operator: Evidence for altered protein and DNA structures in the complex, *Biochemistry 33*, 10701−10710.
23. Warshaw, M. M., and Cantor, C. R. (1970) Oligonucleotide interactions. IV. Conformational differences between deoxy- and ribodinucleoside phosphates, *Biopolymers 9*, 1079−1103.
24. Kallansrud, G., and Ward, B. (1996) A comparison of measured and calculated single- and double-stranded oligodeoxynucleotide extinction coefficients, *Anal. Biochem. 236*, 134−138.
25. Thomas, G. J., Jr., and Barylski, J. (1970) Thermostating capillary cells for a laser-Raman spectrophotometer, *Appl. Spectrosc. 24*, 463−464.
26. Movileanu, L., Benevides, J. M., and Thomas, G. J., Jr. (1999) Temperature dependence of the Raman spectrum of DNA. I. Raman signatures of premelting and melting transitions of poly(dA-dT)·poly(dA-dT), *J. Raman Spectrosc. 30*, 637−649.
27. Thomas, G. J., Jr., Benevides, J. M., and Prescott, B. (1986) DNA and RNA structures in crystals, fibers and solutions by Raman spectroscopy with applications to nucleoproteins, in *Biomolecular Stereodynamics* (Sarma, R. H., and Sarma, M. H., Eds.) Vol. IV, pp 227−253, Adenine Press, Guilderland, NY.
28. Benevides, J. M., Wang, A. H. J., van der Marel, G. A., van Boom, J. H., and Thomas, G. J., Jr. (1988) Crystal and solution structures of the *B*-DNA dodecamer d(CGCAAATTTGCG) probed by Raman spectroscopy: Heterogeneity in the crystal structure does not persist in the solution structure, *Biochemistry 27*, 931−938.
29. Thomas, G. J., Jr., and Wang, A. H. J. (1988) Laser Raman spectroscopy of nucleic acids, in *Nucleic Acids & Molecular Biology* (Eckstein, F., and Lilley, D. M. J., Eds.) Vol. 2, pp 1−30, Springer-Verlag, Berlin.
30. Thomas, G. J., Jr., and Tsuboi, M. (1993) Raman spectroscopy of nucleic acids and their complexes, in *Advances in Biophysical Chemistry* (Bush, C. A., Ed.) Vol. 3, pp 1−70, JAI Press, Greenwich, CT.
31. Deng, H., Bloomfield, V. A., Benevides, J. M., and Thomas, G. J., Jr. (1999) Dependence of the Raman signature of genomic *B*-DNA on nucleotide base sequence, *Biopolymers 50*, 656−666.
32. Yoon, C., Privé, G. G., Goodsell, D. S., and Dickerson, R. E. (1988) Structure of an alternating B-DNA helix and its relationship to A-tract DNA, *Proc. Natl. Acad. Sci. U.S.A. 85*, 6332−6336.
33. Nelson, H. C., Finch, J. T., Luisi, B. F., and Klug, A. (1987) The structure of an oligo(dA)·oligo(dT) tract and its biological implications, *Nature 330*, 221−226.
34. Privé, G. G., Yanagi, K., and Dickerson, R. E. (1991) Structure of the B-DNA decamer C-C-A-A-C-G-T-T-G-G and comparison with isomorphous decamers C-C-A-A-G-A-T-T-G-G and C-C-A-G-G-C-C-T-G-G, *J. Mol. Biol. 217*, 177−199.
35. Goodsell, D. S., Kopka, M. L., Cascio, D., and Dickerson, R. E. (1993) Crystal structure of CATGGCCATG and its implications for A-tract bending models, *Proc. Natl. Acad. Sci. U.S.A. 90*, 2930−2934.
36. Thomas, G. J., Jr., and Benevides, J. M. (1985) An *A*-helix structure for poly(dA-dT)·poly(dA-dT), *Biopolymers 24*, 1101−1105.
37. Movileanu, L., Benevides, J. M., and Thomas, G. J., Jr. (2002) Temperature dependence of the Raman spectrum of DNA. II. Raman signatures of premelting and melting transitions of poly(dA)·poly(dT) and comparison with poly(dA-dT)·poly(dA-dT), *Biopolymers 63*, 181−194.
38. Cann, J. R., Pfenninger, O., and Pettijohn, D. E. (1995) Theory of the mobility-shift assay of nonspecific protein-DNA complexes governed by conditional probabilities: The HU:DNA complex, *Electrophoresis 16*, 881−887.
39. Surette, M. G., Buch, S. J., and Chaconas, G. (1987) Transpososomes: Stable protein-DNA complexes involved in the in vitro transposition of bacteriophage Mu DNA, *Cell 49*, 253−262.
40. Benevides, J. M., Weiss, M. A., and Thomas, G. J., Jr. (1991) DNA recognition by the helix-turn-helix motif: Investigation by laser Raman spectroscopy of the phage λ repressor and its interaction with operator sites O_L1 and O_R3, *Biochemistry 30*, 5955−5963.
41. Duguid, J. G., Bloomfield, V. A., Benevides, J. M., and Thomas, G. J., Jr. (1995) Raman spectroscopy of DNA-metal complexes. II. The thermal denaturation of DNA in the presence of Sr^{2+}, Ba^{2+}, Mg^{2+}, Ca^{2+}, Mn^{2+}, Co^{2+}, Ni^{2+}, and Cd^{2+}, *Biophys. J. 69*, 2623−2641.
42. Duguid, J., Bloomfield, V. A., Benevides, J., and Thomas, G. J., Jr. (1993) Raman spectroscopy of DNA-metal complexes. I. Interactions and conformational effects of the divalent cations: Mg, Ca, Sr, Ba, Mn, Co, Ni, Cu, Pd, and Cd, *Biophys. J. 65*, 1916−1928.
43. Aubrey, K. L., Casjens, S. R., and Thomas, G. J., Jr. (1992) Secondary structure and interactions of the packaged dsDNA genome of bacteriophage P22 investigated by Raman difference spectroscopy, *Biochemistry 31*, 11835−11842.
44. Overman, S. A., Aubrey, K. L., Reilly, K. E., Osman, O., Hayes, S. J., Serwer, P., and Thomas, G. J., Jr. (1998) Conformation and interactions of the packaged double-stranded DNA genome of bacteriophage T7, *Biospectroscopy 4*, S47−S56.
45. Erfurth, S. C., Bond, P. J., and Peticolas, W. L. (1975) Characterization of the A → B transition of DNA in fibers and gels by laser Raman spectroscopy, *Biopolymers 14*, 1245−1257.
46. Benevides, J. M., and Thomas, G. J., Jr. (1983) Characterization of DNA structures by Raman spectroscopy: High-salt and low-salt forms of double helical poly(dG-dC) in H_2O and D_2O solutions and application to *B*, *Z* and *A*-DNA, *Nucleic Acids Res. 11*, 5747−5761.
47. Peticolas, W. L., and Evertsz, E. (1992) Conformation of DNA in vitro and in vivo from laser Raman scattering, *Methods Enzymol. 211*, 335−352.
48. Thomas, G. J., Jr., Benevides, J. M., Overman, S. A., Ueda, T., Ushizawa, K., Saitoh, M., and Tsuboi, M. (1995) Polarized Raman spectra of oriented fibers of A DNA and B DNA: Anisotropic and isotropic local Raman tensors of base and backbone vibrations, *Biophys. J. 68*, 1073−1088.
49. Prescott, B., Steinmetz, W., and Thomas, G. J., Jr. (1984) Characterization of DNA structures by laser Raman spectroscopy, *Biopolymers 23*, 235−256.
50. Tsuboi, M., Komatsu, K., Hoshi, J., Kawashima, E., Sekine, T., Ishido, Y., Russell, M. P., Benevides, J. M., and Thomas, G. J., Jr. (1997) Raman and infrared spectra of (2′*S*)-[2′-^{2}H] thymidine: Vibrational coupling between deoxyribosyl and thymine moieties and structural implications, *J. Am. Chem. Soc. 119*, 2025−2032.
51. Serban, D., Benevides, J. M., and Thomas, G. J., Jr. (2002) DNA secondary structure and Raman markers of supercoiling in *Escherichia coli* plasmid pUC19, *Biochemistry 41*, 847−853.
52. Nishimura, Y., Tsuboi, M., Sato, T., and Aoki, K. (1986) Conformation-sensitive Raman lines of mononucleotides and their

use in a structure analysis of polynucleotides: Guanine and cytosine nucleotides, *J. Mol. Struct. 146*, 123−153.
53. Miura, T., and Thomas, G. J., Jr. (1994) Structural polymorphism of telomere DNA: Interquadruplex and duplex-quadruplex conversions probed by Raman spectroscopy, *Biochemistry 33*, 7848−7856.
54. Laporte, L., and Thomas, G. J., Jr. (1998) A hairpin conformation for the 3′ overhang of *Oxytricha nova* telomeric DNA, *J. Mol. Biol. 281*, 261−270.
55. Claret, L., and Rouviere-Yaniv, J. (1997) Variation in HU composition during growth of *Escherichia coli*: The heterodimer is required for long-term survival, *J. Mol. Biol. 273*, 93−104.
56. Balandina, A., Kamashev, D., and Rouviere-Yaniv, J. (2002) The bacterial histone-like protein HU specifically recognizes similar structures in all nucleic acids. DNA, RNA, and their hybrids, *J. Biol. Chem. 277*, 27622−27628.
57. Werner, M. H., Huth, J. R., Gronenborn, A. M., and Clore, G. M. (1995) Molecular basis of human 46X,Y sex reversal revealed from the three-dimensional solution structure of the human SRY-DNA complex, *Cell 81*, 705−714.
58. Love, J. J., Li, X., Case, D. A., Giese, K., Grosschedl, R., and Wright, P. E. (1995) Structural basis for DNA bending by the architectural transcription factor LEF-1, *Nature 376*, 791−795.
59. Sheflin, L. G., Fucile, N. W., and Spaulding, S. W. (1993) The specific interactions of HMG 1 and 2 with negatively supercoiled DNA are modulated by their acidic C-terminal domains and involve cysteine residues in their HMG 1/2 boxes, *Biochemistry 32*, 3238−3248.
60. Hardman, C. H., Broadhurst, R. W., Raine, A. R., Grasser, K. D., Thomas, J. O., and Laue, E. D. (1995) Structure of the A-domain of HMG1 and its interaction with DNA as studied by heteronuclear three- and four-dimensional NMR spectroscopy, *Biochemistry 34*, 16596−16607.
61. Lavoie, B. D., Shaw, G. S., Millner, A., and Chaconas, G. (1996) Anatomy of a flexer-DNA complex inside a higher-order transposition intermediate, *Cell 85*, 761−771.
62. Shindo, H., Furubayashi, A., Shimizu, M., Miyake, M., and Imamoto, F. (1992) Preferential binding of *E. coli* histone-like protein HU alpha to negatively supercoiled DNA, *Nucleic Acids Res. 20*, 1553−1558.
63. Pinson, V., Takahashi, M., and Rouviere-Yaniv, J. (1999) Differential binding of the *Escherichia coli* HU, homodimeric forms and heterodimeric form to linear, gapped and cruciform DNA, *J. Mol. Biol. 287*, 485−497.
64. Dame, R. T., and Goosen, N. (2002) HU: Promoting or counteracting DNA compaction?, *FEBS Lett. 529*, 151−156.
65. Wen, Z. Q., and Thomas, G. J., Jr. (1998) Ultraviolet resonance Raman spectroscopy of DNA and protein constituents of viruses: Assignments and cross sections for excitations at 257, 244, 238 and 229 nm, *Biopolymers 45*, 247−256.
66. Schultz, S. C., Shields, G. C., and Steitz, T. A. (1991) Crystal structure of a CAP-DNA complex: The DNA is bent by 90°, *Science 253*, 1001−1007.
67. Kukolj, G., and DuBow, M. S. (1992) Integration host factor activates the Ner-repressed early promoter of transposable Mu-like phage D108, *J. Biol. Chem. 267*, 17827−17835.
68. Kamashev, D., Balandina, A., and Rouviere-Yaniv, J. (1999) The binding motif recognized by HU on both nicked and cruciform DNA, *EMBO J. 18*, 5434−5444.
69. Benevides, J. M., Terwilliger, T. C., Vohník, S., and Thomas, G. J., Jr. (1996) Raman spectroscopy of the Ff gene V protein and complexes with poly(dA): Nonspecific DNA recognition and binding, *Biochemistry 35*, 9603−9609.

BI030050R